J Inorg Organomet Polym (2017) 27:552–561
DOI 10.1007/s10904-017-0497-9

Ultrasound-Assisted Synthesis of a Novel Nano-Zigzag-Pattern Lead (II) Metal–Organic System: A New Precursor to Produce Nano-Sized PbO

Younes Hanifehpour[1] · Teng Zhou[2] · Babak Mirtamizdoust[3] · Hossein Mostaanzadeh[3] · Sang Woo Joo[1]

Received: 26 October 2016 / Accepted: 3 January 2017 / Published online: 27 January 2017

Abstract A sonochemical method was used to synthesize a new nano Pb(II) 1D metal–organic zigzag chain $[Pb(p\text{-}2\text{-einh})NO_2]_n$ (**1**) (p-2-einh = (1-(pyridin-2-yl)ethylidene) isonicotinohydrazide). The compound was characterized by scanning electron microscopy (SEM), transmission electron microscopy, elemental analysis, IR spectroscopy, thermogravimetric analysis, X-ray powder diffraction, and single-crystal X-ray analysis. The X-ray analysis reveals a 1D zigzag-chain metal–organic polymer structure for **1** that is further extended to a 3D supramolecular structure by—interaction and other labile interactions. A coordination number of six was determined for the Pb(II) ions in PbN_3O_3. Lead oxide nanoparticles were prepared at 180 °C by thermolysis of **1**. The average diameter of the nanoparticles was 20 nm. The size and morphology of the PbO samples were observed using SEM, and the structure of the system was optimized by DFT calculations. The calculated structural parameters and FT-IR spectra are consistent with the crystal structure.

Keywords Nano metal–organic system · Ultrasonic irradiation · Zigzag chain · Nano PbO

1 Introduction

In recent years, metal–organic coordination systems have attracted much attention due to their diverse characterization in areas such as catalysis, gas storage, membranes separations, medical imaging, and drug delivery. These polymers are formed by an automatic self-assembly process. One of the methods of producing coordination polymers is binding organic ligands to metal ions to create a chain or network [1–4].

Metal–organic coordination polymer systems are very similar to organic polymers except that they have metallic ions or clusters in their cores instead of carbon. Metal–organic coordination systems can have one, two, or three-dimensional forms. The materials used in the synthesis process are of great importance for the structure of the synthesized coordination polymers. Crystalline materials with excellent properties are mostly synthesized via methods such as solvothermal, diffusion, gel-diffusion, volatilization, and surfactant thermal methods. Various types of metal–organic coordination systems with diverse structures and properties can be produced by using different coordination groups [5–11].

There has been interest in synthesizing metal–organic coordination polymers of Pb(II), which is related to the *s* orbitals of lead because of the inert pair effect [12]. Lead is an environmental pollutant with dangerous toxic effects, and it can change the structure of RNA because it binds perfectly to thiol and phosphate groups in nucleic acids. Lead has played an important role in industry. It is used in paints and in the construction of batteries because it is

Teng Zhou has equal contribution as the first author.

✉ Younes Hanifehpour
y_hanifehpour@yu.ac.kr

✉ Sang Woo Joo
swjoo@yu.ac.kr

Teng Zhou
zhou.teng@live.com

[1] School of Mechanical Engineering, Yeungnam University, Gyeongsan 712-749, South Korea

[2] Mechanical and Electrical Engineering College, Hainan University, Haikou 570228, Hainan Province, People's Republic of China

[3] Department of Chemistry, Faculty of Science, University of Qom, PO Box 37185-359, Qom, Iran

Scheme 1 Synthesis of Hp-2-einh

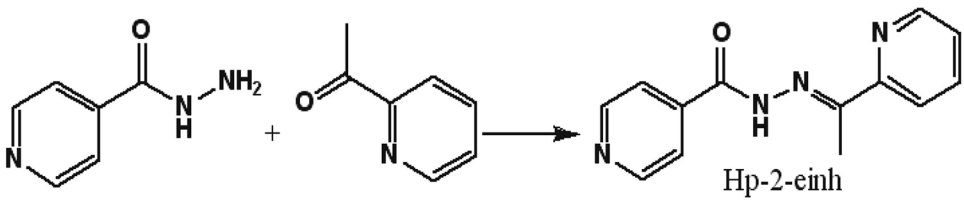

cheap. It was even used in fuels to improve the octane number and anti-knock properties [2–16].

Our attention is focused on the design and synthesis of Pb(II) coordination compounds, and we have recently reported various nano Pb(II) coordination polymers [17–33]. In this paper, we report a new asymmetrical Pb(II) metal–organic coordination system using p-2-einh Schiff-base ligand with a nitrite counter ion. We describe a simple sonochemical synthetic method for the preparation of nanostructures of this metal–organic coordination polymer and its use in the preparation of lead oxide nanoparticles.

2 Experimental

2.1 Materials and Physical Measurements

The ligand Hp-2-einh (1-(pyridin-2-yl)ethylidene)isonicotinohydrazide was synthesized according to a previously reported method [34]. The chemicals were obtained from Sigma-Aldrich (Seoul, South Korea) and used as received without further purification. Elemental analyses of the samples were carried out using a Vario Microanalyzer. IR spectra were recorded on a Bruker Vector 22 FT-IR spectrometer using KBr disks in the range of 4000–400 cm^{-1}. Thermogravimetric analysis (TGA) and differential scanning calorimetry (DSC) curves were recorded on a SETARAM LABSYS Thermal Analyzer under N_2 flow in the temperature range of 25–800 °C with a heating rate of 3°C/min.

X-ray powder diffraction (XRD) measurements were done using an X'pert diffractometer (Panalytical) with monochromatized Cu-k_α radiation. XRD powder patterns based on single crystal data were obtained using Mercury simulations [35]. The morphology of the nanostructured compound was determined by scanning electron microscopy (SEM) (S-4200, Hitachi, Japan) and transmission electron microscopy (JEM-2200FS, JEOL Ltd., Japan). Ultrasonic irradiation was applied for 1 h with a multiwave ultrasonic generator (Sonicator_3000, Misonix Inc., Farmingdale, NY, USA) equipped with a converter/transducer and a 12.5-mm-diameter titanium oscillator (horn) operating at room temperature and 20 kHz with a maximum power output of 600 W.

2.2 Synthesis of (1-(pyridin-2-yl)ethylidene) isonicotinohydrazidede (Hp-2-einh)

According to Scheme 1, a mixture of isonicotinohydrazide (1.37 g, 10 mmol) and a solution of 1-(pyridin-2-yl)ethanone (1.22 mL, 10 mmol) in methanol (100 mL) was refluxed for 24 h. The resulting white solid was filtered off, washed with methanol, and vacuum dried (yield: 87%). M.p. 158 °C.

IR υ_{max}; υ_{max}(626, 724, 749, 789, 1123, 1150, 1216, 1382, 1457, 1494, 1550, 1579, 1623, 1670, 3071, 3301) cm^{-1} (KBr) [34].

2.3 Preparation of Single Crystal and Nanostructure of $[Pb(p\text{-}2\text{-}einh)NO_2]_n$ (1)

Nanostructures of $[Pb(p\text{-}2\text{-}einh)NO_2]_n$ (**1**) were prepared by adding 30 mL of a 0.1 M solution of the Hp-2-einh ligand and 30 mL of a 0.1 M solution of $NaNO_2$ to 30 mL of a 0.1 M solution of $Pb(CH_3COO)_2$ in water. This mixture was subjected to sonication using a high-density ultrasonic probe operating at 20 kHz and 600 W. The obtained precipitates were filtered off, washed with water, and dried in air.

Product 1: d.p. = 398 °C. Analysis: Found; C: 32.00, H: 3.00, N: 14.30%. Calculated for $C_{13}H_{11}N_5O_3Pb$: C: 31.71, H: 2.25, N: 14.22%.

FT-IR (selected bands, in cm^{-1}): 650 *m*, 655 *m*, 690 *m*, 855 *m*, 1026 *m*, 1140 *m*, 1322 *m*,1381 *s*, 1598 *s*, 1639 *s*, 2989 *m*, 3012 *w*.

To prepare and isolate single crystals of $[Pb(p\text{-}2\text{-}einh)NO_2]_n$ (**1**) for X-ray structure determination, 1 mmol of Hp-2-einh and $NaNO_2$ was placed in one arm of a branched tube [36], and 1 mmol of $Pb(CH_3COO)_2$·(0.07 g) was placed in the other arm. Methanol was then carefully added to fill both arms. The tube was sealed, the ligand-containing arm was immersed in an oil bath at 60 °C, and the other arm was left at ambient temperature. Yellow crystals (d.p. 395 °C) were deposited in the arm at ambient temperature after 3 days. They were filtered off, washed with acetone and ether, and air-dried (yield: 83%).

Found; C: 32.00, H: 3.00, N: 14.30%. Calculated for $C_{13}H_{11}N_5O_3Pb$: C: 31.71, H: 2.25, N: 14.22%.

FT-IR (selected bands, in cm^{-1}): 652 *m*, 655 *m*, 691 *m*, 855 *m*, 1025 *m*, 1140 *m*, 1322 *m*,1381 *s*, 1598 *s*, 1639 *s*, 2989 *m*, 3015 *w*.

Table 1 Crystal data and structure refinement for $[Pb(p\text{-}2\text{-einh})NO_2]_n$ (**1**)

Chemical formula	$C_{13}H_{11}N_5O_3Pb$
M_r	492.46
Crystal system, space group	Monoclinic, $P2_1/n$
Temperature (K)	179
a, b, c (Å)	8.1660 (11), 13.2850 (17), 13.7842 (18)
β (°)	92.860 (4)
V (Å^3)	1493.5 (3)
Z	4
Radiation type	λ = 0.71073 Å
μ (mm^{-1})	11.32
Crystal size (mm)	0.21 × 0.14 × 0.11
Absorption correction	Multi-scan *SADABS* V2008/1 (Bruker AXS)
T_{min}, T_{max}	0.20, 0.37
No. of measured, independent and observed [$I > 2\sigma(I)$] reflections	18486, 3318, 2666
R_{int}	0.051
$(\sin\theta/\lambda)_{max}$ (Å^{-1})	0.646
$R[F^2 > 2\sigma(F^2)]$, $wR(F^2)$, S	0.029, 0.073, 0.96
No. of reflections	3318
No. of parameters	200
H-atom treatment	H-atom parameters constrained
$\Delta\rangle_{max}$, $\Delta\rangle_{min}$ (e Å^{-3})	2.35, −1.21

2.4 Synthesis of Pb(II) Oxide Nanoparticles

A light yellow solution was formed after dissolving 0.1 mmol of $[Pb(p\text{-}2\text{-einh})NO_2]_n$ (**1**) in 10 mL of oleic acid. This solution was degassed for 30 min and then heated to 180 °C for 2 h. Finally, a black precipitate was formed at the end of the reaction. A large excess of ethanol and a small amount of toluene were added to the solution, and PbO nanoparticles were separated by centrifugation. The final solids were washed with ethanol and dried in ambient air (yield: 63%).

2.5 Crystallography

A crystal of the compound (yellow, parallelepiped, dimensions: 0.21 × 0.14 × 0.11 mm) was mounted on glass fiber with epoxy adhesive. Data were collected using an X-ray diffractometer (SMART APEX II, Bruker) with graphite-monochromated Mo K_α radiation (λ = 0.71073 Å) at 50 kV and 30 mA over a 2θ range of 7.34°–52.00°. No significant decay was observed during the data collection.

The data were processed using the Bruker AXS Crystal Structure Analysis Package [37]. The following modules of the AXS package were used: data collection: APEX2 (Bruker, 2010); cell refinement: SAINT (Bruker, 2009); data reduction: SAINT (Bruker, 2009); absorption correction: SADABS (Bruker, 2008); structure solution: XPREP (Bruker, 2008), and SHELXS-97 (Sheldrick, 2008); structure refinement: SHELXL-97 (Sheldrick, 2008); molecular graphics and publication materials: SHELXTL (Sheldrick, 2008). The scattering factors of neutral atoms were obtained from Waber and Cromer [38]. The sample underwent phase transition at a low temperature, so the data were collected at room temperature.

The crystal has a monoclinic space group $P2_1/m$ based on the systematic absences, E statistics, and successful refinement of the structure. The structure was solved by direct methods. Full-matrix least-square refinements minimizing the function $\sum w\,(F_o^{\,2} - F_c^{\,2})^2$ were applied to the data acquired from the compound. The non-hydrogen atoms were refined anisotropically. All H atoms were placed in geometrically calculated positions with C–H = 0.95 (aromatic) and 0.98(CH_3) Å and refined as riding atoms with Uiso(H) = 1.5UeqC(CH_3) or 1.2 UeqC(other C). Tables 1 and 2 show the crystallographic data, bond lengths, and angles.

2.6 Computational Details

The geometry of the input structure of complex 1 (Scheme 2) was optimized using a B3LYP density functional model [39, 40]. In these calculations, we used the 6-311++G** basis set for all carbon, nitrogen, oxygen, and hydrogen atoms. The LanL2DZ valence and effective

Table 2 Selected bond lengths (Å) and angles (°) for [Pb(p-2-einh)NO_2]$_n$ (**1**)

	Experimental	Calculated		Experimental	Calculated
Pb1–O1	2.386 (4)	2.302	Pb1–N2	2.462 (4)	2.423
Pb1–O3	2.387 (4)	2.303	Pb1–N1	2.585 (4)	2.569
Pb1–O2	2.767	2.791	Pb1–N4^{i}	2.486 (4)	2.490
O1–Pb1–O3	82.35 (14)	82.44	O1–Pb1–N1	78.04 (13)	78.10
O1–Pb1–N2	75.03 (13)	75.12	O3–Pb1–N1	128.83 (12)	129.00
O3–Pb1–N2	65.45 (13)	66.76	N2–Pb1–N1	63.95 (13)	65.26

Scheme 2 Materials produced and synthetic methods

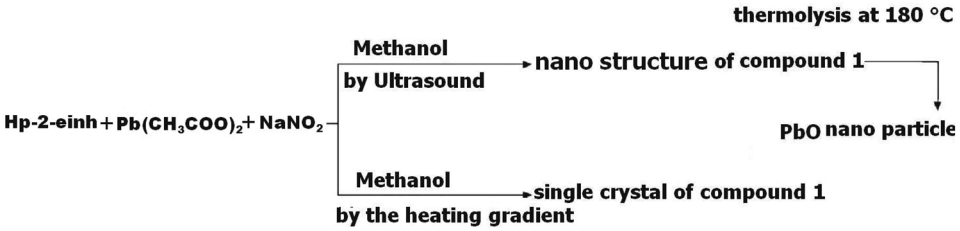

core potential functions were used for the lead atom [41].[1] All DFT calculations were performed using the Gaussian 09 software package [43]. Electron levels such as the lowest unoccupied molecular orbital (LUMO) energy, highest occupied molecular orbital (HOMO) energy, and frontier molecular orbital coefficients were calculated. Molecular sketches of all compounds were drawn using Gauss View 03 [44]. Natural bond orbital (NBO) analysis was applied to determine the atomic charges [45].

3 Results and Discussion

The reaction of the p-2-einh ligand with Pb$(CH_3COO)_2$·and $NaNO_2$ led to the formation of the new Pb(II) metal–organic polymer [Pb(p-2-einh)NO_2]$_n$ (**1**). Nanostructures of compound **1** were obtained by ultrasonication in a methanolic solution, and a single-crystalline sample was obtained using a heat gradient applied to a solution of the reagents (the branched tube method [36]). Scheme 3 gives an overview of the methods used for the synthesis of [Pb(p-2-einh)NO_2]$_n$ (**1**) using the two different routes.

The IR spectrum and elemental analysis of the single-crystalline material and nanostructure are identical. Selected spectral data and the corresponding data acquired from DFT calculations are provided in Table 3. The FT-IR spectra of the single-crystalline materials and the nanostructures show characteristic absorption bands of the Hp-2-einh ligand. The relatively weak band around 3012 cm^{-1} is attributed to the absorption of aromatic CH hydrogen

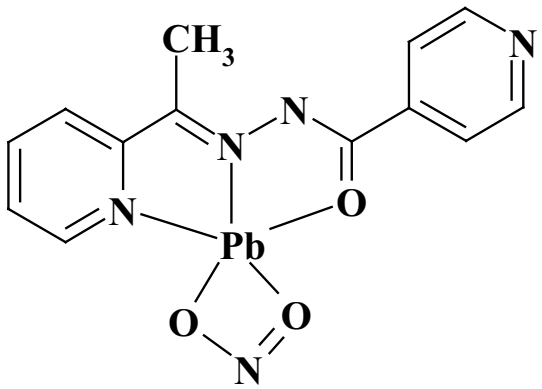

Scheme 3 Input structure of compound **1**

Table 3 Experimental FT-IR frequencies (cm^{-1}) for [Pb(p-2-einh)NO_2]$_n$ compared with the theoretical frequencies obtained from DFT calculations

Assignment	Experimental	Calculated
ν (C–H)$_{aliphatic}$	2989 *m*	3028.6
ν (C–H)$_{aromatic}$	3012 *w*	3149.6
δ (C–H)	655 *m*	577.5
ν (CC)$_{rings\ vibration}$	1381–1598 *s*	1347.3–1630.7
ν (NO_2)	1322 *m*	1433.3
ν (CO)	1639 *s*	1532.4
ν (Pb–N)$_{pyridine}$	650 *m*	649.3
ν (Pb–N)$_{aliphatic}$	690 *m*	687.9
ν (Pb–O)$_{carbonyl}$		435.6
ν (Pb–O)$_{nitrite}$		275.5

[1] A description of the basis sets and theory level used in this work can be found in the following: [42].

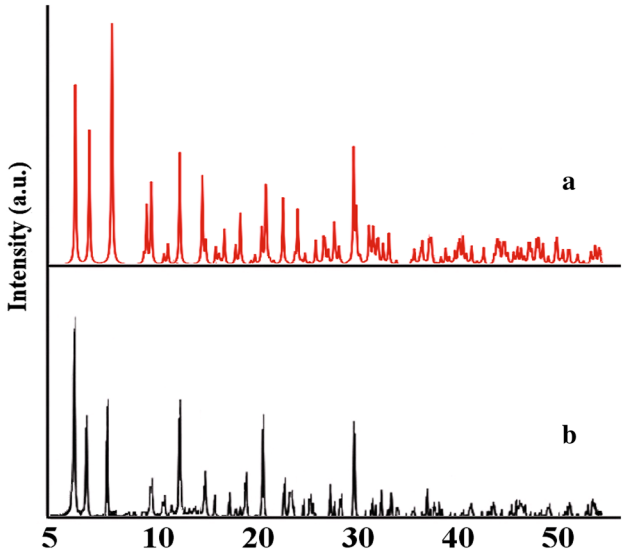

Fig. 1 XRPD patterns **a** computed from single-crystal X-ray data of compound **1, b** nano-structure of compound **1**

atoms, and the band around 2989 cm^{-1} is attributed to the absorption of aliphatic CH hydrogen atoms. The vibrations aromatic rings of the Hp-2-einh ligand occurred in the frequency range of 1381–1598 cm^{-1}. The band at 1322 cm^{-1} is due to NO_2^- stretching vibration.

Figure 1a shows the XRD pattern of compound **1** simulated from single-crystal X-ray data. Figure 1b shows the experimental XRD pattern of compound **1** prepared by the sonochemical process. The experimental and simulated powder X-ray diffraction patterns show only slight differences in 2 values (Fig. 1b. This shows that the compound obtained by the sonochemical route is almost identical to the single crystalline sample. The average grain size was estimated as 37 nm using the Scherrer formula ($D = 0.891\lambda/\beta\cos\theta$, where D is the average grain size, λ is the X-ray wavelength (0.15405 nm), β is the diffraction angle of an observed peak, and is its full-width at half-maximum).

Figure 2 shows the nanostructures observed by SEM. Interestingly, the morphology of compound **1** prepared by the sonochemical method (Fig. 2) is composed of hexagonal nanoplates with thickness of 25–40 nm. The TEM image and SAED patterns of compound **1** confirm the hexagonal plate morphology and its crystallinity (Fig. 3).

Further investigation required for explanation of the mechanism of formation of these structures. However, the supramolecular structure of the compound may influence. The morphology of nanostructured compound can be affected by the packing of the structure on a molecular level [28, 46–48] (Fig. 4).

Based on single-crystal X-ray crystallography (Table 1), the structure of $[Pb(p\text{-}2\text{-}einh)NO_2]_n$ crystallizes in a

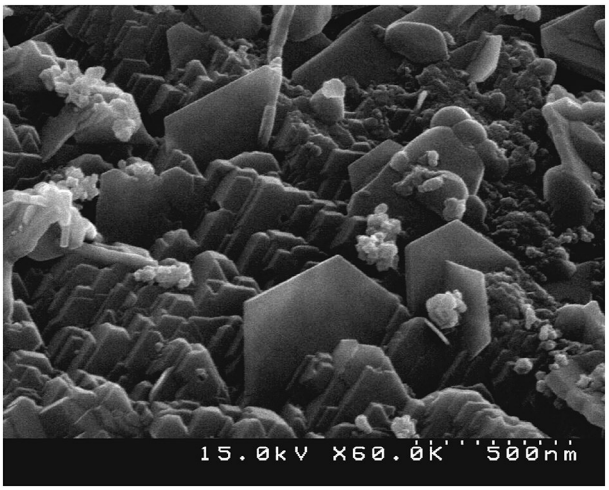

Fig. 2 SEM photographs of $[Pb(p\text{-}2\text{-}einh)NO_2]_n$ (**1**) nanostructures

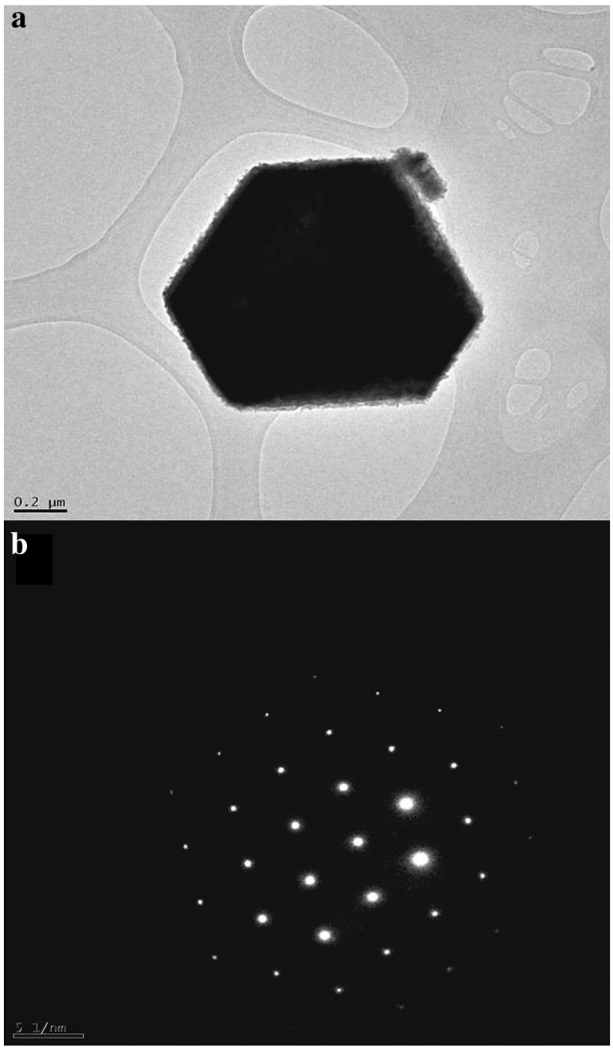

Fig. 3 TEM photographs of $[Pb(p\text{-}2\text{-}einh)NO_2]_n$ (**1**) nano-plates

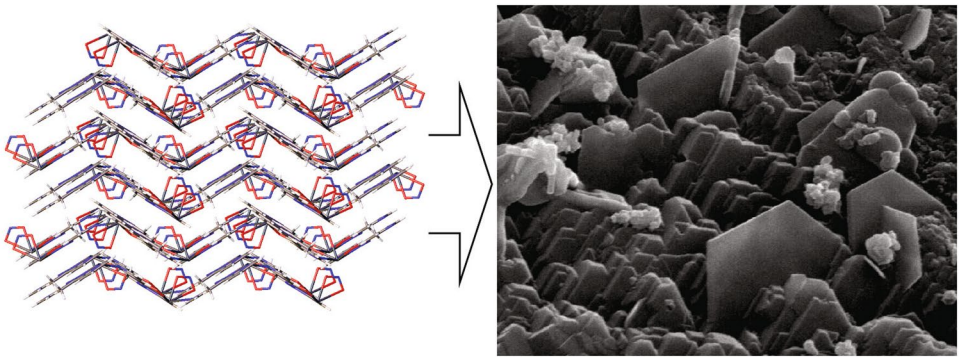

Fig. 4 Left: packing of the structure at a molecular level; Right: morphology of the nano-structure

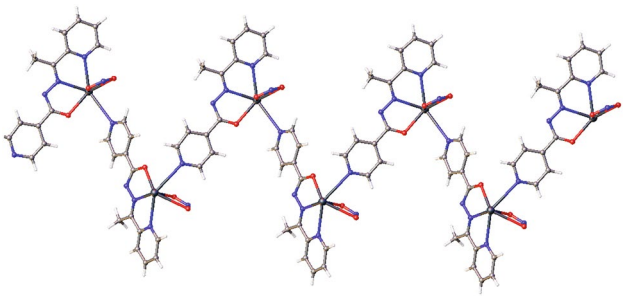

Fig. 5 Fragment of the coordination polymer showing the 1D zigzag metal–organic polymer

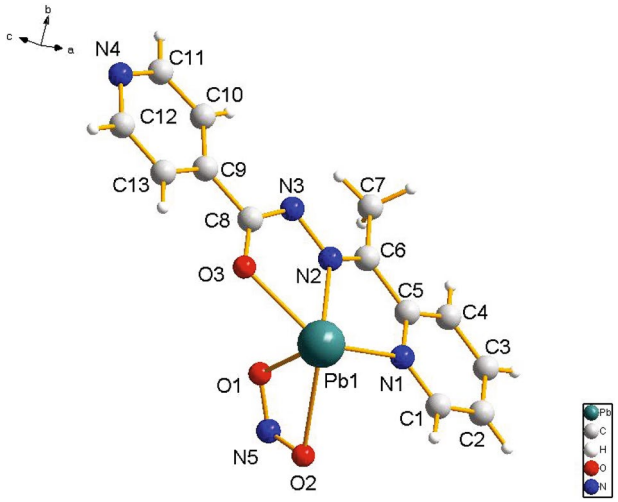

Fig. 6 Molecular asymmetrical unit of $[Pb(p\text{-}2\text{-}einh)NO_2]_n$ (**1**) [the coordination sphere of Pb1 center is not completed]

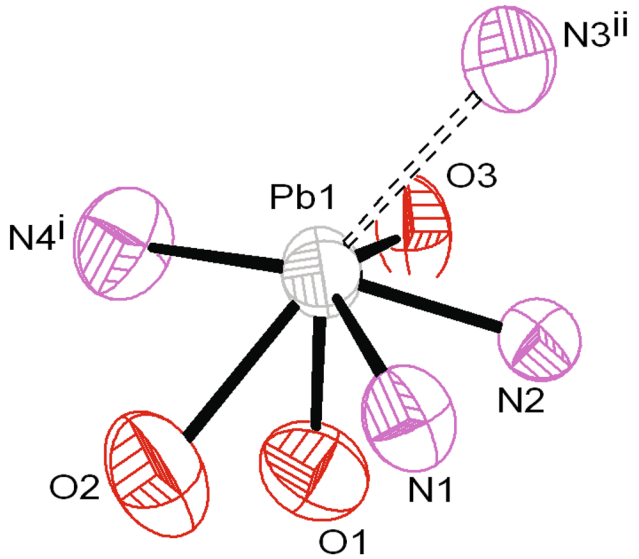

Fig. 7 Schematic representation of Pb(II) environment

monoclinic system with space group $P2_1/n$, taking the form of a one-dimensional zigzag metal–organic polymer in the solid state (Fig. 5). Figure 6 shows the asymmetrical unit structure of **1** and a selected atom numbering scheme.

Figure 7 shows that the Pb(II) atom is coordinated by three nitrogen atoms of two "p-2-einh" ligands with Pb–N distances of 2.462 (4), 2.585 (4), and 2.486 (4) Å; one oxygen atom of "p-2-einh" with Pb–O distance of 2.767 Å; and two oxygen atoms of two coordinated nitrite ligands with Pb–O distances of 2.761 (4) and 2.388 (4) Å in a three fashion with a PbN_3O_3 donor set. Therefore, the coordination number of the Pb(II) atom is six with asymmetrical geometry.

This order suggests a gap or hole in the coordination geometry around the metal ions that is possibly occupied by a stereo-active lone pair of electrons on Pb(II) [49]. The observed shortening of the Pb–O bonds on the side of the Pb^{2+} ion opposite to the putative lone pair supports this possibility (2.386 (3) Å compared with 2.886 (4) Å adjacent to the lone pair) [49]. This environment provides space for close contact with other atoms in many Pb(II) compounds [49, 50]. We found a strong interaction between $N3^{ii}$ of the p-2-einh ligand and the Pb center in this structure ($Pb\text{-}N3^{ii} = 3.237(7)$, see Fig. 7). This results in short distances between Pb–N that are close to that

Table 4 Selected non-covalent contacts in the crystal structure of 1

C–H···O	H···O Å	H···C Å	<O···H–C°
C12–H12···O2	2.573	3.201	133.62
C4–H4···O2	2.655	3.011	105.29
C12–H12···O2	2.572	3.201	133.62

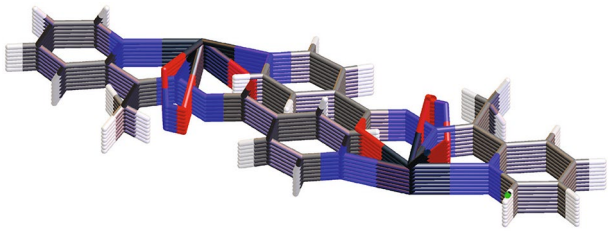

Fig. 8 Projection of the nearest neighbor pairs' – stacks of heteroaromatic bases in $[Pb(p\text{-}2\text{-}einh)NO_2]_n$ (**1**)

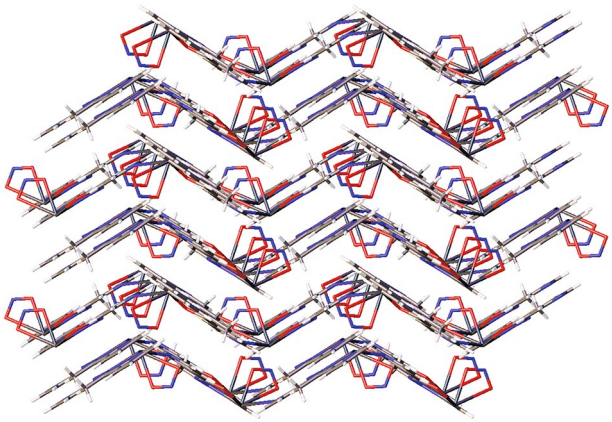

Fig. 9 From 1D architecture to supramolecular 3D polymer via labile interactions

of a covalent bond. The C–H…O interactions are usually classified as weak non-covalent bonding between adjacent atoms. However, the observed distance values for these interactions (Table 4) suggest relatively strong interaction between these atoms [40].

As shown in Fig. 8, there is an interaction between the Pb(II) and a N5 from a neighboring chain. In the structure – stacking interactions observed between the parallel aromatic rings belonging to adjacent chains. The interplanar distance of the aromatic rings are 3.552 Å, that are noticeably shorter than the normal – stacking [50] onsequence, labile interactions also allow the 1D zigzag molecular architecture to interact with neighboring chains and to extend the structure to a 3D supramolecular architecture (Figs. 9, 10)

Thus, the coordination sphere of Pb(II) ions in this complex may be controlled by the labile and lone pair activity and – stacking interactions. The lone pair activity or stacking interactions may cause ligand stacking, while the cooperative effect of the – interactions and the presence of the lone pair are responsible for closer packing of the solved structure.

To evaluate the thermal stability of complex **1**, TGA and differential thermal analysis were carried out between 20 and 800 °C in an argon flow (Fig. 11). The compound **1** was stable up to 348 °C, at which a decomposition process started. Based on the XRD pattern, the final product upon thermal decomposition of compound **1** is PbO.

3.1 DFT Calculations

The optimized structure is shown in Fig. 12 and Table 2 indicates the calculated structural parameters. The experimental data are for the solid phase, whereas the calculated data correspond to the isolated molecules in the gas phase. The computational and experimental data in Table 2 clearly display that they differ only slightly from each other. For instance, the largest difference between the experimental and calculated Pb1–O1 length is about 0.084 Å, while the largest deviation of the O3–Pb1–N2 angle is 1.32°.

Table 3 presents the computed IR frequencies and experimentally determined frequencies. The assignment of the ν(Pb–O) vibrations is based on the theoretically calculated frequency with values of 435 and 275 cm^{-1} for Pb(II) complex $[Pb(p\text{-}2\text{-}einh)NO_2]_n$. The NBO charges were also calculated in the case of Pb(II) and the coordinated atoms. The positive charge of the Pb(II) ions was 1.348. The charges of the coordinated nitrogen atoms of the "p-2-einh" ligands were −0.544, −0.364, and −0.443, respectively. The charges of the coordinated oxygen atoms of nitrite were −0.578 and −0.463, while that of the coordinated oxygen atom of the "p-2-einh" ligands was −0.788. The calculations show that complex **1** has 108 occupied molecular orbitals (MOs) per $[Pb(p\text{-}2\text{-}einh)NO_2]_n$ unit.

The energy separation between the HOMO and LUMO was also computed, as shown in Fig. 13. The HOMO is mainly localized on four nitrogen atoms and one oxygen atom of the "p-2-einh" ligand and two oxygen atoms of the nitrite anion including Pb(II). The LUMO is approximately delocalized on all atoms of the "p-2-einh" ligand. The HOMO–LUMO gap is 3.423 eV.

3.2 PbO Nanoparticles

PbO nanoparticles were prepared by the decomposition of precursor **1** in oleic acid as a surfactant at 180 °C under an air atmosphere. Figure 14 shows the XRD pattern of the PbO nanoparticles. All the peaks can be attributed to

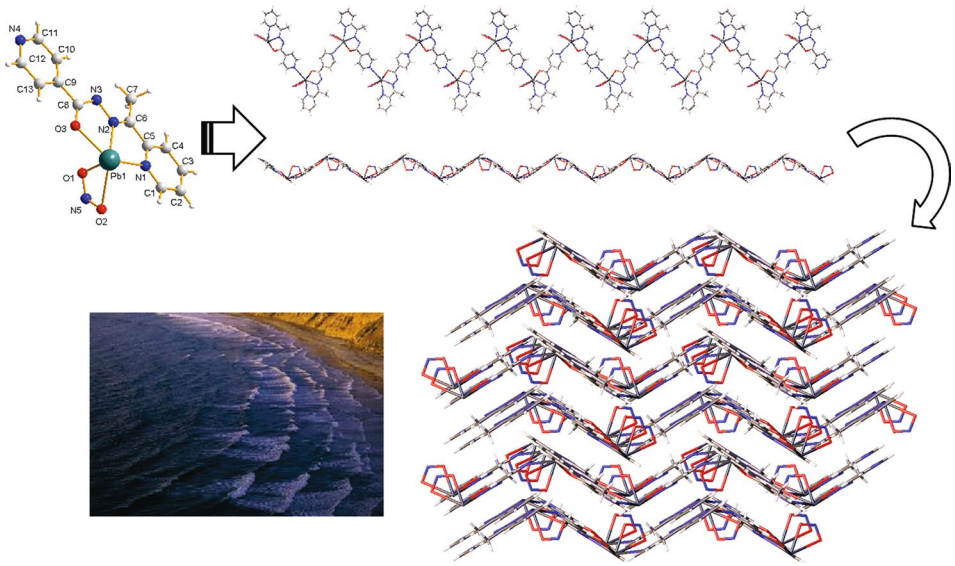

Fig. 10 Transition from discrete architecture to supramolecular 3D zigzag metal–organic polymer

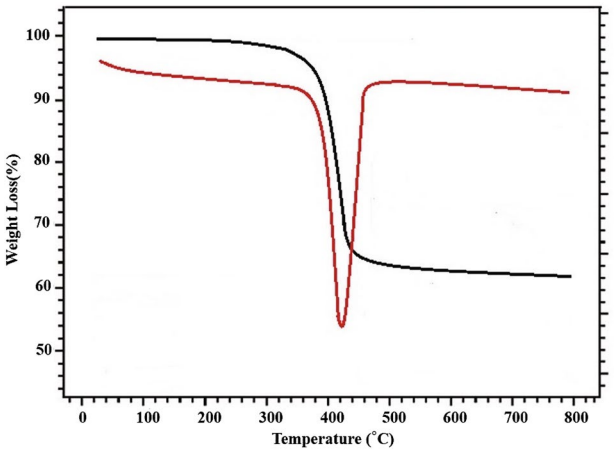

Fig. 11 TGA and DTG plot for $[Pb(p\text{-}2\text{-}einh)NO_2]_n$ (**1**)

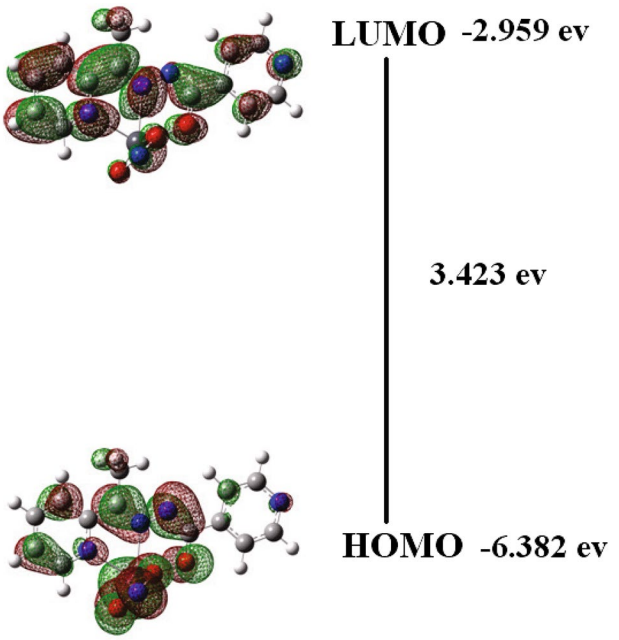

Fig. 13 Frontier molecular orbitals for a unit of $[Pb(p\text{-}2\text{-}einh)NO_2]_n$ (**1**)

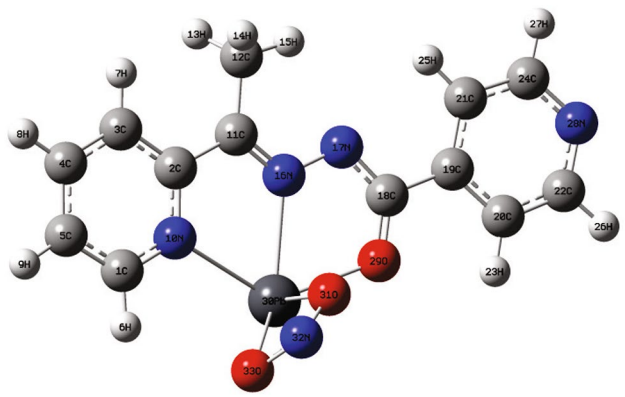

Fig. 12 Optimized molecular structure of compound **1**

a cubic structure with a lattice parameter of a = 5.9143(4) Å, which is consistent with the standard data file (JCPDS No: 78-1897).

The size and morphology of the PbO samples were further evaluated using SEM. A regular shape of the Pb(II) oxide nanoparticles was observed (Fig. 15). The size distribution of the PbO particles was in the range of 8–45 nm.

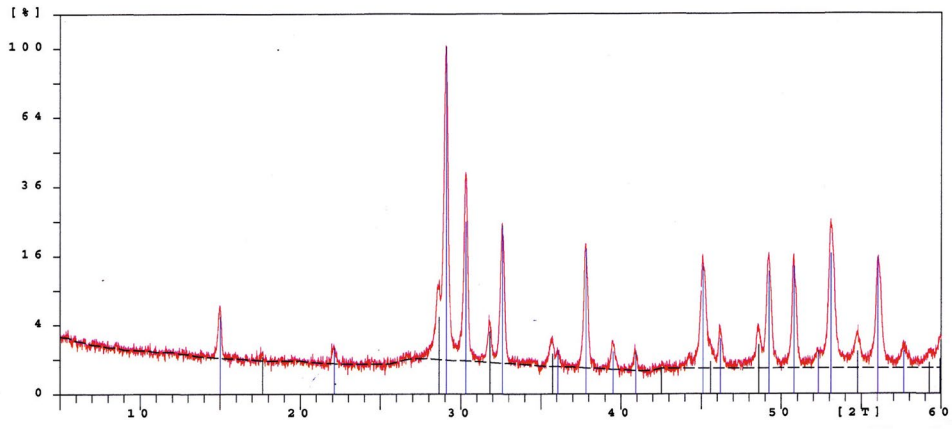

Fig. 14 XRD pattern PbO prepared after thermolysis of compound [Pb(p-2-einh)NO2] n (**1**)

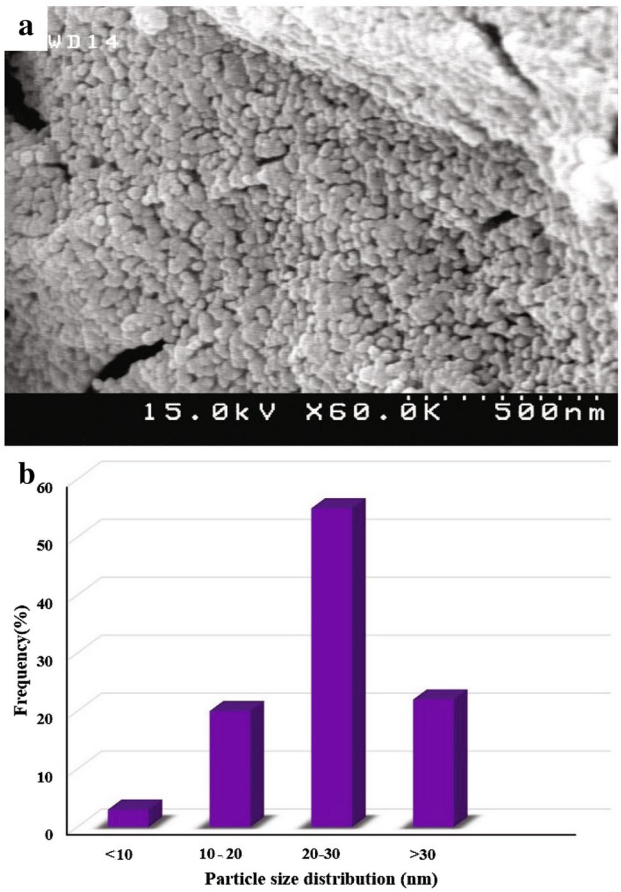

Fig. 15 **a** SEM photograph of PbO nano-structures (produced by thermolysis of nanostructures) and **b** size distribution of PbO nanoparticles

4 Conclusion

A novel nano Pb(II) 1D zigzag metal–organic polymer containing (1-(pyridin-2-yl)ethylidene)isonicotinohydrazide ligand was synthesized by a sonochemical for the first time. The morphology of sonochemically prepared **1** is composed of nanoplates with thickness of 25–40 nm. The complex takes the form of a one-dimensional zigzag metal–organic polymer in the solid state, and the 1D structure extends to a 3D supramolecular coordination polymer through several labile interactions with neighboring chains. The computed bond distances, angles, and vibrational frequencies from DFT calculations are in good agreement with the experimental data. Uniform PbO nanoparticles were obtained by thermolysis of compound 1.

5 Supplementary Material

Crystallographic data for the structures reported in this paper have been deposited at the Cambridge Crystallographic Data Centre as supplementary publication CCDC-1439396 for $[Pb(p\text{-}2\text{-}einh)NO_2]_n$ (**1**). Copies of the data can be obtained from the CCDC, 12 Union Road, Cambridge CB2 1EZ, UK (Fax: +441223336033, e-mail: deposit@ccdc.cam.ac.uk).

Acknowledgements Support for this investigation from the University of Qom is gratefully acknowledged. This work is funded by Yeungnam University Postdoctoral Fellowship Program.

References

1. R. Chakrabarty, P.S. Mukherjee, P.J. Stang, Chem. Rev. **111**, 6810 (2011)
2. A. Erxleben, Coord. Chem. Rev. **246**, 203 (2003)
3. C.L. Cahill, D.T. de Lill, M. Frisch, CrystEngComm. **9**, 15 (2007)
4. A. Morsali, L.-G. Zhu, Helv. Chim. Acta **89**, 81 (2006)
5. S.R. Batten, S.M. Neville, D.R. Turner, Coordination Polymers: Design, Analysis and Application (Royal Society of Chemistry, Cambridge, 2009)
6. C. Janiak, Dalton Trans. **2003**, 2781
7. K. Akhbari, A. Morsali, Dalton. Trans. **42**, 4786 (2013)
8. T. Uemura, S. Kitagawa, Chem. Lett. **34**,132 (2005)
9. N. Soltanzadeh, A. Morsali, Ultrason. Sonochem. **17**, 139 (2010)

10. H. Sadeghzadeh, A. Morsali, CrystEngComm. **12**, 370 (2010)
11. W. Lu, S.S.-Y. Chui, K.-M. Ng, C.-M. Che, Angew. Chem.Int. Ed. **47**, 4568 (2008)
12. L. Shimonni-Livny, J.P. Glusker, C.W. Bock, Inorg. Chem. **37**, 1853 (1998)
13. J. Parr, Polyhedron **16**, 551 (1997)
14. S. Sobanska, J. P. Wignacourt, P. Conflant, M. Drache, M. Lagrenee, E.M. Holt, New J. Chem. **23**, 393 (1999)
15. E.J. Baran, C.C. Wagner, M. Rossi, Z.F. Caruso, Anorg. Allg. Chem. **626**, 701 (2000)
16. B. Mirtamizdoust, Z. Trávníček, Y. Hanifehpour, P. Talemi, H. Hammud, S.W. Joo, Ultrason. Sonochem. **34**, 255 (2015)
17. B. Mirtamizdoust, D. Bieńko, Y. Hanifehpour, E.R.T. Tiekink, V.T. Yilmaz, P. Talemi, S.W. Joo, J. Inorg. Organomet. Polym. **26**, 819 (2016)
18. A. Valipour, B. Mirtamizdoust, M. Ghaedi, F. Taghizadeh, P. Talemi, J. Inorg. Organomet. Polym. **26**, 197 (2016)
19. B. Shaabani, B. Mirtamizdoust, D. Viterbo, G. Croce, H. Hammud, P. Hojati-Lalemi, Z.A. Khandar, Anorg. Allg. Chem. **637**, 713 (2011)
20. B. Mirtamizdoust, B. Shaabani, S.W. Joo, D. Viterbo, G. Croce, Y. Hanifehpour, J. Inorg. Organomet. Polym. **22**, 1397 (2012)
21. B. Shaabani, B. Mirtamizdoust, M. Shadman, H.K. Fun, Z. Anorg. Allg. Chem. **635**, 2642 (2009)
22. B. Mirtamizdoust, B. Shaabani, A. Khandar, H.K. Fun, S. Huang, M. Shadman, P. Hojati-Talemi, Z. Anorg. Allg. Chem. **638**, 844 (2012)
23. Y. Hanifehpour, B. Mirtamizdoust, S.W. Joo, J. Inorg. Organomet. Polym. **22**, 916 (2012)
24. Y. Hanifehpour, B. Mirtamizdoust, A.R. Farzam, S.W. Joo, J. Inorg. Organomet. Polym. **22**, 957 (2012)
25. B. Mirtamizdoust, S. Ali-Asgari, S.W. Joo, E. Maskani, Y. Hanifehpour, T.H. Oh, J. Inorg. Organomet. Polym. **23**, 751 (2013)
26. Y. Hanifehpour, A. Morsali, B. Mirtamizdoust, S.W. Joo, J. Mol. Struct. **1079**, 67 (2015)
27. B. Mirtamizdoust, M.S. Shalamzari, S. Behrouzi, M.H. Florencio, H.K. Fun, J. Inorg. Organomet. Polym. **22**, 1358 (2012)
28. Y. Hanifehpour, B. Mirtamizdoust, A. Morsali, S.W. Joo, Ultrason. Sonochem. **23**, 275 (2015)
29. Y. Hanifehpour, B. Mirtamizdoust, A. Morsali, S.W. Joo, Ultrason. Sonochem. **31**, 201–205 (2016)
30. G.H. Shahverdizadeh, F. Hakimi, B. Mirtamizdoust, A. Soudi, P. Hojati-Talemi, J. Inorg. Organomet. Polym. **22**, 903 (2012)
31. Y. Hanifehpour, V. Safarifard, A. Morsali, B. Mirtamizdoust, S.W. Joo, Ultrason. Sonochem. **23**, 282 (2015)
32. Y. Hanifehpour, B. Mirtamizdoust, B. Khomami, S.W. Joo, Z. Anorg. Allg. Chem. **641**, 2466 (2015)
33. Y. Hanifehpour, B. Mirtamizdoust, M. Hatami, B. Khomami, S.W. Joo, J. Mol. Struct. **1091**, 43 (2015)
34. M.R. Maurya, S. Khurana, W. Zhang, D. Rehder, J. Chem. Soc. Dalton Trans. **3015** (2003)
35. Mercury 1.4.1, Copyright Cambridge Crystallographic Data Centre, 12 Union Road, Cambridge, CB2 1EZ, UK, 2001–2005
36. J.M. Harrowfield, H. Miyamae, B.W. Skelton, A.A. Soudi, A.H. White, Aust. J. Chem **49**, 1165 (1996)
37. Bruker AXS Crystal Structure Analysis Package: Bruker (2000). SHELXTL. Version 6.14. Bruker AXS Inc., Madison, Wisconsin, USA. Bruker (2008). SADABS. Version 2008/1. Bruker AXS Inc., Madison, Wisconsin, USA. Bruker (2008). XPREP. Version 2008/2. Bruker AXS Inc., Madison, Wisconsin, USA. Bruker (2009). SAINT. Version 7.68 A. Bruker AXS Inc., Madison, Wisconsin, USA. Bruker (2010). APEX2. Version 2010.3–0. Bruker AXS Inc., Madison, Wisconsin, USA
38. D.T. Cromer, J.T. Waber, International Tables for X-ray Crystallography, vol. 4 (Kynoch Press, Birmingham, 1974), **Table 2.2 A**
39. A.D. Becke, J. Chem. Phys. **98**, 5648 (1993)
40. A. Lee, W. Yang, R.G. Parr, Phys. Rev. B **37**, 785 (1988)
41. P.J. Hay, W.R. Wadt, J. Chem. Phys. **82**, 270 (1985)
42. J.B. Foresman, A.E. Frisch, Exploring Chemistry with Electronic Structure Methods, 2nd ed. (Gaussian Inc., Pittsburgh, 1996)
43. Gauss View, Version 3.0 Gaussian Inc., Pittsburgh, 2003
44. A.E. Reed, F. Weinhold, Chem. Rev. **88**, 899 (1998)
45. H.B. Schelegel, Ab Initio Methods in Quantum Chemistry (Wiley, New York, 1987), pp. 249–286
46. L. Hashemi, A. Morsali, Ultrason. Sonochem **24**, 146 (2015)
47. K. Akhbari, S. Beheshti, A. Morsali, G. Bruno, H. Amiri Rudbari, Inorg. Chim. Acta **423**, 101 (2014)
48. L. Hashemi, A. Morsali, Ultrason. Sonochem. **21**, 1417 (2014)
49. L. Shimoni-Livny, J.P. Glusker, C.W. Brock, Inorg. Chem. **37**, 1853 (1998)
50. C.A. Hunter, J.K.M. Sanders, J. Am. Chem. Soc. **112**, 5525 (1990)